Kinetic Pathways of Phase Ordering in Lipid Raft Model Systems

Jian Liu,[†,‡] Jay T. Groves,[†,‡,§] and Arup K. Chakraborty*[,†,‡,§,∥,⊥]

Department of Chemistry, Department of Chemical Engineering, Biophysics Graduate Group, University of California, Berkeley, California 94720, and Physical Biosciences and Materials Sciences Division, Lawrence Berkeley National Laboratory, Berkeley, California 94720

Received: August 27, 2005; In Final Form: January 30, 2006

We studied kinetic pathways of order−order transitions in bilayer lipid mixtures using a time-dependent Ginzburg−Landau (TDGL) approach. During the stripe-to-hexagonal phase transition in an incompressible two-component system, the stripe phase first develops a pearl-like instability along the phase boundaries, which grows and drives the stripes to break up into droplets that arrange into a hexagonal pattern. These dynamic features are consistent with recent experimental observations. During the disorder-to-hexagonal phase transition in an incompressible three-component system, the disordered state first passes through a transient stripelike structure, which eventually breaks up into a hexagonal droplet phase. Our results suggest experiments with synthetic vesicles where the stripelike patterns could be observed.

Introduction

Lipid rafts are domains with a distinct lipid and protein composition in cell membranes. These enigmatic structures are approximately 100 nm in size and are enriched in sphingolipids, cholesterols, and certain membrane proteins. It has been suggested that lipid rafts are implicated in cellular signaling events.[1−4] Though still controversial, lipid rafts are widely thought to originate from phase transitions of lipid immiscibility. An interesting driving force of phase separation in two dimensions is the coupling between the local membrane concentration and the spontaneous curvature difference.[5] Such a force is clearly visible in many synthetic lipid raft membrane systems,[6−9] where domains of the size of about 1 μm (or bigger) are observed. However, it is difficult to reconcile the much smaller size of lipid rafts on living cell membranes by this driving force.

Recently, we have suggested that electrostatic interactions between membrane components may provide the additional driving force that is required to determine the size of lipid rafts on living cell membranes.[10] In this paper, we first studied the dynamics of order−order phase transition for an incompressible two-component lipid mixture where the origin of the long-ranged interactions is either electrostatic or curvature coupling to concentration fluctuation. We found that both models yield qualitatively the same phase ordering dynamics, where a pearling instability occurs during the stripe-to-hexagonal-droplet phase transition. This predicted dynamic feature is commensurate with the recent experimental observations by Rozvosky et al.[11] The difference between the two models is in the length and the time scales characterizing domain formation. We also studied the dynamics of the order−disorder phase transition for an incompressible three-component lipid raft model system, where long-ranged electrostatic interactions are important for domain formation. A nontrivial dynamic pathway is predicted; upon temperature quenching, the system in the disordered state will first pass through a stripelike morphology which then breaks into droplet phases by a pearling instability.

This paper is organized as follows. The thermodynamic models, the dynamic equations, and the simulation methods are presented in section II. The results are discussed in section III. We offer concluding remarks in section IV.

Theory Development and Models

1. Two-Component Incompressible Lipid Raft Model System. *Model 1: Electrostatic Interactions.* We model the membrane as a flat, two-dimensional manifold, which consists of lipid raft component A and nonraft component B. Each component carries different effective dipole moments aligned in a direction normal to the membrane. The dipolar interaction could come from the effective electrostatic interactions of the net charges on the surfaces of synthetic vesicles or from the dipole moments of transmembrane proteins.[10,12] The following free energy functional describes the thermodynamics of such a system:

$$F = \int \mathrm{d}\vec{x}_1 \int \mathrm{d}\vec{x}_2 \frac{D^2 \psi(\vec{x}_1)\,\psi(\vec{x}_2)}{(\vec{x}_1 - \vec{x}_2)^3} + \int \mathrm{d}\vec{x} \left\{ \frac{1}{2}\gamma(\nabla\psi(\vec{x}))^2 + \frac{1}{2}\tau_0 \psi(\vec{x})^2 + A_3\psi(\vec{x})^3 + A_4\psi(\vec{x})^4 \right\} \quad (1)$$

The order parameter, ψ, is defined as $\psi = \rho_A - \bar{\rho}_A$; it characterizes the extent to which the components are spatially segregated (when $\psi = 0$, the components are uniformly distributed). Here, ρ_i is the density of species i; $\bar{\rho}_i$ is the average density of species i. $D = (d_A - d_B)/(4\pi\epsilon_0\epsilon_{membrane})^{1/2}$ is the effective dipole moment difference between A and B. ϵ_0 is the electric permittivity in a vacuum, the effective dielectric constant of the membrane is $\epsilon_{membrane} = 3$, and d_i is the normal component of the effective dipole moment carried by species i. The line tension, γ, is the free energy penalty for spatial variation of the densities of components, and it attempts to minimize the phase

* Corresponding author. E-mail: arup@uclink.berkeley.edu.
† Department of Chemistry, University of California, Berkeley.
‡ Physical Biosciences, Lawrence Berkeley National Laboratory.
§ Biophysics Graduate Group, University of California, Berkeley.
∥ Department of Chemical Engineering, University of California, Berkeley.
⊥ Materials Sciences Division, Lawrence Berkeley National Laboratory.

10.1021/jp054855f CCC: $33.50
Published on Web 04/04/2006

boundary as much as possible. τ_0 is the phenomenological Flory−Huggins parameter that determines the degree to which the two components are incompatible. It is a combination of entropic and enthalpic interactions between the constituents, depending on the inverse of the temperature. The higher order terms in the order parameter, ψ, are originated in entropy and can be derived from Flory−Huggins formalism to be $A_3 = -(1/6)[(1/\bar{\rho}_A^2) - (1/\bar{\rho}_B^2)]$ and $A_4 = (1/12)[(1/\bar{\rho}_A^3) + (1/\bar{\rho}_B^3)]$.

At high temperatures, entropy dominates over enthalpy, $\tau_0 > 0$; therefore, no ordered phase is preferred. At lower temperatures, $\tau_0 < 0$, and this can lead to a phase segregation, where the balance between the quadratic terms and the higher order terms in (1) results in a finite value of the order parameter, $\psi \neq 0$, at the global free energy minimum. The line tension prefers a macroscopic phase separation which minimizes the energetically unfavorable contacts between the two phases. However, the long-ranged dipolar interactions are repulsive; they prefer small domains. This competition between the line tension and the long-ranged dipolar interactions results in an optimal finite domain size at thermodynamic equilibrium. In the weak segregation limit, this optimal finite domain size corresponds to the inverse of the optimal wavenumber, $2\pi/q^*$, for concentration fluctuations, where $q^* = D^2/2\gamma$. Under normal experimental conditions for synthetic vesicles, $D \sim 1$ D/nm^2 and $\gamma \sim k_BT$, which give rise to the optimal domain size ~300 nm.

For a conserved order parameter, the phase ordering dynamics is governed by the model B type time-dependent Ginzburg−Landau equation:[13]

$$\frac{\partial\psi(\vec{x},t)}{\partial t} = M\nabla^2\frac{\delta F[\psi(\vec{x},t)]}{\delta\psi(\vec{x},t)} + \xi(\vec{x},t) \qquad (2)$$

Here, the order parameter fields evolve according to the gradients of the free energy functional. M is the mobility coefficient, which we assume to be a constant; $\xi(\vec{x},t)$ is a random noise, which satisfies the fluctuation−dissipation relation at temperature T, $\langle\xi(\vec{x}_1,t_1)\ \xi(\vec{x}_2,t_2)\rangle = -2Mk_BT\nabla^2\delta(\vec{x}_1 - \vec{x}_2)\ \delta(t_1 - t_2)$. In Fourier space, eq 2 becomes

$$\frac{\partial\hat{\psi}}{\partial t} = M(-k^2\hat{G} - \gamma k^4\hat{\psi} + D^2k^3\hat{\psi} - \tau k^2\hat{\psi}) + \hat{\xi}(\vec{k},t) \quad (3)$$

where $G = A_3\psi^3 + A_4\psi^4$ in real space and $\hat{G}$ is G's counterpart in Fourier space. τ consists of τ_0 and the average repulsive dipolar interactions.

Model 2: Spontaneous Curvature Differences Coupled to Concentration Fluctuations. The free energy functional for a system where the components prefer different spontaneous curvatures is as follows:

$$F = \int d\vec{x}\left\{\frac{1}{2}\gamma(\nabla\psi(\vec{x}))^2 + \frac{1}{2}\tau\psi(\vec{x})^2 + A_3\psi(\vec{x})^3 + A_4\psi(\vec{x})^4 + \frac{1}{2}\sigma(\nabla h(\vec{x}))^2 + \frac{1}{2}\kappa(\nabla^2 h(\vec{x}))^2 + S\psi\nabla^2 h\right\} \quad (4)$$

The order parameter, ψ, the line tension, γ, Flory−Huggins parameter, τ, A_3, and A_4 are the same as those in model 1. For simplicity, we model the membrane as a relatively flat two-dimensional manifold. $h(\vec{x})$ is the membrane height fluctuation in Monge gauge,[14] σ is the surface tension of the membrane, κ is the bending rigidity, $S = (H_A - H_B)\kappa$, and H_i is the spontaneous curvature for pure species i. If the membrane fluctuates on much faster time scales than the time scale over which the concentration fields change, we can average over the membrane height fluctuations exactly and obtain an effective free energy as we did in a previous paper.[10] Then, the optimal domain size for this model is determined by $2\pi/q^*$, where $q^* = \{[S(\sigma/\gamma)^{1/2} - \sigma]/\kappa\}^{1/2}$. We choose the parameters as follows: $\gamma = 4k_BT$,[15,16] $\kappa = 40k_BT$,[15,17] $\sigma = 3.1 \times 10^{-6}$ N/m,[17] and $H_A - H_C \approx 1.0\ \mu m^{-1}$;[6,7,11,18] with these parameters, an optimal domain size of ~1.2 μm is obtained.

The phase ordering dynamics is given by

$$\frac{\partial\psi(\vec{x},t)}{\partial t} = M_\psi\nabla^2\frac{\delta F[\psi(\vec{x},t),h(\vec{x},t)]}{\delta\psi(\vec{x},t)} + \xi(\vec{x},t) \qquad (5)$$

$$\frac{\partial h(\vec{x},t)}{\partial t} = M_h\nabla^2\frac{\delta F[\psi(\vec{x},t),h(\vec{x},t)]}{\delta h(\vec{x},t)} + \eta(\vec{x},t) \qquad (6)$$

$\langle\xi(\vec{x}_1,t_1)\ \xi(\vec{x}_2,t_2)\rangle = -2M_\psi k_BT\nabla^2\delta(\vec{x}_1 - \vec{x}_2)\ \delta(t_1 - t_2)$, and $\langle\eta(\vec{x}_1,t_1)\ \eta(\vec{x}_2,t_2)\rangle = -2M_h k_BT\nabla^2\delta(\vec{x}_1 - \vec{x}_2)\ \delta(t_1 - t_2)$. Although we did not specify the vesicle topology in our model, we treated the membrane height fluctuation, h, as a conserved field because the volume and surface area are approximately constant in recent experiments with lipid vesicles.[11]

2. Three-Component Incompressible Lipid Raft Model System. *Model 3: Three Components with Electrostatic Interactions.* Lipid raft formation is much more complicated than the phase transitions of a binary system. For example, in living cells, there is evidence that there are at least three distinct species involved in lipid raft formation.[19,20] Here, we consider a generic system consisting of a lipid raft component, a nonraft component, and a background lipid. [Note that the "three components" refer to three incompatible entities (each entity could be a composite of more than one chemical component), that can lead to a three-phase region in the phase diagram. In usual experiments with synthetic systems, the three components (sphingolipids, cholesterols, and phospholipids) are actually two incompatible components in terms of phase transitions in that sphingolipids and cholesterols act as one entity that segregates from phospholipids.]

We have previously derived the free energy functional for a three-component system with electrostatic interactions[10] to be

$$F = \int d\vec{x}_1\int d\vec{x}_2\sum_{i,j}^{A,B}\frac{D_iD_j\psi_i(\vec{x}_1)\ \psi_j(\vec{x}_2)}{(\vec{x}_1 - \vec{x}_2)^3} + \frac{1}{2}\int d\vec{x}\{(\gamma_A + \gamma_C)(\nabla\psi_A(\vec{x}))^2 + (\tau_A^{(0)} + \tau_C^{(0)})\psi_A(\vec{x})^2 + (\gamma_B + \gamma_C)(\nabla\psi_B(\vec{x}))^2 + (\tau_B^{(0)} + \tau_C^{(0)})\psi_B(\vec{x})^2 + (2\gamma_C)(\nabla\psi_A(\vec{x}))\cdot(\nabla\psi_B(\vec{x})) + 2\tau_C^{(0)}\psi_A(\vec{x})\ \psi_B(\vec{x})\}\int d\vec{x}\{A_3\psi_A(\vec{x})^3 + B_3\psi_B(\vec{x})^3 - C_3(\psi_A(\vec{x}) + \psi_B(\vec{x}))^3 + A_4\psi_A(\vec{x})^4 + B_4\psi_B(\vec{x})^4 + C_4(\psi_A(\vec{x}) + \psi_B(\vec{x}))^4\} \quad (7)$$

The order parameters are $\psi_i(\vec{x}) = [\rho_i(\vec{x}) - \bar{\rho}_i]/\rho_{total}$ and $\rho_{total} = \sum_i \rho_i = 1$, and $\bar{\rho}_i$ is the average concentration for species i. The dipole moment differences are $D_A = (d_A - d_C)/(4\pi\epsilon_0\epsilon_{membrane})^{1/2}$ and $D_B = (d_B - d_C)/(4\pi\epsilon_0\epsilon_{membrane})^{1/2}$. $A_3 = -(1/6)(1/\bar{\rho}_A^2)$, $B_3 = -(1/6)(1/\bar{\rho}_B^2)$, $C_3 = -(1/6)(1/\bar{\rho}_C^2)$, $A_4 = (1/12)(1/\bar{\rho}_A^3)$, $B_4 = (1/12)(1/\bar{\rho}_B^3)$, $C_4 = (1/12)(1/\bar{\rho}_C^3)$. As a minimal model, we also assume the line tensions are the same, $\gamma_A = \gamma_B = \gamma_C = \gamma$. Except for three components in the system instead of two components, the basic physics for model 3 is the same as that of model 1. On the basis of our previous calculations,[10] in the weak segregation limit, if we choose $D_A = 8$ D/nm^2, $D_B = 1$ D/nm^2, and $\gamma = 5.0k_BT$, the raft domains that form are of the order of 50 nm.

The time evolution of the order parameter fields are dictated by the time-dependent Ginzburg−Landau (TDGL) equations:

$$\frac{\partial \psi_A(\vec{x},t)}{\partial t} = M_A \nabla^2 \frac{\delta F[\psi_A(\vec{x},t),\psi_B(\vec{x},t)]}{\delta \psi_A(\vec{x},t)} + \xi_A(\vec{x},t) \quad (8)$$

$$\frac{\partial \psi_B(\vec{x},t)}{\partial t} = M_B \nabla^2 \frac{\delta F[\psi_A(\vec{x},t),\psi_B(\vec{x},t)]}{\delta \psi_B(\vec{x},t)} + \xi_B(\vec{x},t) \quad (9)$$

$\langle \xi_A(\vec{x}_1,t_1)\, \xi_A(\vec{x}_2,t_2)\rangle = -2Mk_BT\nabla^2\delta(\vec{x}_1 - \vec{x}_2)\, \delta(t_1 - t_2)$, $\langle \xi_A(\vec{x}_1,t_1)\, \xi_A(\vec{x}_2,t_2)\rangle = -2Mk_BT\nabla^2\delta(\vec{x}_1 - \vec{x}_2)\, \delta(t_1 - t_2)$, and $\langle \xi_A(\vec{x}_1,t_1)\, \xi_B(\vec{x}_2,t_2)\rangle = 0$. We choose the same time scales for A and B ($M_A = M_B = M$) and the same magnitude for the noise levels ξ_A and ξ_B. After Fourier transformation, the equations become

$$\frac{\partial \hat{\psi}_A}{\partial t} = M(-k^2\hat{G}_A - 4\gamma k^4\hat{\psi}_A + D_A{}^2k^3\hat{\psi}_A - (\tau_A + \tau_C)k^2\hat{\psi}_A - 2\gamma k^4\hat{\psi}_B + D_AD_Bk^3\hat{\psi}_B - \tau_Ck^2\hat{\psi}_B) + \hat{\xi}_A(\vec{k},t) \quad (10)$$

$$\frac{\partial \hat{\psi}_B}{\partial t} = M(-k^2\hat{G}_B - 4\gamma k^4\hat{\psi}_B + D_B{}^2k^3\hat{\psi}_B - (\tau_B + \tau_C)k^2\hat{\psi}_B - 2\gamma k^4\hat{\psi}_A + D_AD_Bk^3\hat{\psi}_A - \tau_Ck^2\hat{\psi}_A) + \hat{\xi}_B(\vec{k},t) \quad (11)$$

$G_A = 3A_3\psi_A{}^2 - 3C_3(\psi_A + \psi_B)^2 + 4A_4\psi_A{}^3 + 4C_4(\psi_A + \psi_B)^3$ and $G_B = 3B_3\psi_B{}^2 - 3C_3(\psi_A + \psi_B)^2 + 4B_4\psi_B{}^3 + 4C_4(\psi_A + \psi_B)^3$ in real space. τ_i consists of the bare Flory−Huggins parameter, $\tau_i^{(0)}$, and the related average repulsive dipolar interactions. We also assume for simplicity that $\tau_A = \tau_B = \tau_C = \tau$.

3. Numerical Simulation Methods. We adopt the semi-implicit Fourier-spectral first-order method[21] to numerically solve the dynamic equations. Taking model 1 as an example, we evolved the system on a 128 × 128 square lattice with periodic boundary conditions. At a given time, the order parameter fields in both the real space, ψ, and the Fourier space, $\hat{\psi}$, are calculated. The nonlinear term G is computed at each lattice site in real space and then is transformed into Fourier space through fast Fourier transformation (FFT). We put this $\hat{G}$ term back into eq 3, update the order parameter, $\hat{\psi}$, and perform the inverse FFT of $\hat{\psi}$ to obtain the real space value of ψ. We repeat this procedure for many time steps. For all of the simulations performed in this paper, the time step is taken to be d$t = 0.0001$. The order parameter, ψ, is plotted on the 128 × 128 square lattices using gray scales.

Results and Discussion

Model 1. We study the dynamics of the transition from the stripe phase to the hexagonal droplet phase. To compare with recent experiments, we impose a temperature jump and a slow drift of the composition, as these are the pertinent experimental conditions.[11] The values of the line tension and dipole moment difference between membrane components are taken to be $\gamma = 4.0k_BT$[15,16] and $D = 0.8$ D/nm^2,[22,23] and they are representative of experimental conditions. A stripe sinusoidal wave in the order parameter, ψ, is first set as the initial condition with the wave vector chosen according to the minimum of the quadratic coefficient in the free energy. The system is then equilibrated over 100 000 time steps at $\tau = -0.2$ and $\rho_A = 0.325$ and subjected to small random noise. Under these conditions, the stable phase is the stripe phase. Starting from this well-equilibrated stripe phase, we suddenly raise the temperature to $\tau = 0.004$ and gradually change the composition from $\rho_A = 0.325$ to $\rho_A = 0.245$, where the rate of change of compositions is chosen to be 0.000 001 per simulation time step in accord with the experimental conditions.[11] This drives the system into a region of the phase diagram where the stable phase is the hexagonal droplet phase ($\tau = 0.004$, $\rho_A = 0.245$).

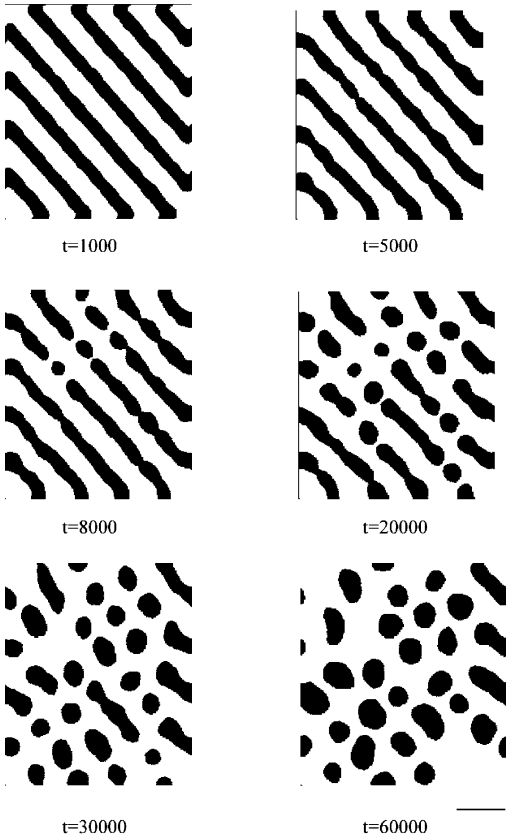

Figure 1. Time evolution of the concentration field for an incompressible two-component lipid raft model system upon temperature jump and composition changes. The phase ordering dynamics is based on a lipid raft formation mechanism, where long-ranged dipolar interaction is dominant. The dark regions are lipid raft domains. t is the simulation time. The temperature jump is instantaneous, from $\tau = -0.2$ to $\tau = 0.004$. The composition is gradually changed from $\rho_A = 0.325$ to $\rho_A = 0.245$. The rate of change of composition is 0.000 001 per simulation time step. The line tension is $\gamma = 4.0k_BT$; the dipole moment difference between the raft component and the nonraft component is $D = 0.8$ D/nm^2. The length scale bar is 300 nm.

Figure 1 shows the time evolution of the raft domains in the simulations. The stripes first develop pearl-like instabilities along their phase boundaries. The characteristic wavelength of this instability is about the same as the width of the stripes. As the instabilities grow, the stripes gradually break up into the droplets, which arrange themselves in an apparent hexagonal geometry. The linear size of the stripes and the droplets is about 150−200 nm, consistent with the measured value for the lipid raft domains in recent experiments.[11] We also study the stripe-to-hexagonal phase transition where there is a temperature jump only without any composition changes. The results (not shown) are qualitatively the same as those shown in Figure 1. (Note that it can be shown that the qualitative dynamic features do not depend on the grid size and the system size in our simulations.) Therefore, the dynamic features of the stripe-to-hexagonal phase transition in model 1 for a two-component system are in agreement with experimental observations for synthetic membrane model systems.[11]

The more complicated 3-dimensional version of the pearling instability that occurs during the hexagonal-to-bcc phase transition has been well understood in diblock copolymer systems. The explicit analysis in terms of the most unstable modes of anisotropic fluctuations was elegantly worked out by Qi and Wang.[24] The interpretation of our simple 2-D version of pearling instability (stripe-to-hexagonal phase transition) is readily interpreted in view of their results. During the stripe-to-hexagonal phase transition, as dictated by the free energy functional, the two most unstable anisotropic concentration fluctuation modes ($\vec{q}_2$ and $\vec{q}_3$) are developed, while the concentration fluctuations of the preexisting mode $\vec{q}_1$ (corresponding to the stripe ordered phase in Fourier space) are reduced. These concentration fluctuation modes follow $|\vec{q}_1| = |\vec{q}_2| = |\vec{q}_3| = q^*$ and $\vec{q}_1 + \vec{q}_2 + \vec{q}_3 = 0$, as governed by the symmetry of the free energy functional. Consequently, enhancements of concentration fluctuations are in directions 120° to the stripes' tangent which, together with concentration fluctuation reductions along the stripe tangent direction, lead to the pearling instability in real space. An explicit algebraic derivation of this result is left for future studies.

It has been also suggested that the difference between the dynamics of a conserved order parameter and that of a nonconserved one is not essential in the weak segregation limit, because only a single wavenumber dominates in this regime.[24] Therefore, we believe that the above results may also be applicable to the dynamics of a nonconserved order parameter.

Model 2. In a similar way, we simulated the stripe-to-hexagonal-droplet phase ordering dynamics upon an instantaneous temperature jump ($\tau = -0.25$ to $\tau = -0.01$) and gradual composition changes from $\rho_A = 0.325$ to $\rho_A = 0.245$ for model 2. Striped sinusoidal waves in the order parameter, ψ, and the membrane height field, h, are first introduced as the initial condition with the wave vector chosen according to the minimum of the quadratic coefficient in the free energy. In our simulations, we vary the relative mobility of the dynamics of the concentration fields and that of the membrane fluctuations, M_ψ/M_h, from 0.01 to 10 (keeping $M_\psi = 1.0$). When the membrane fluctuates much faster than the concentration fields ($M_\psi/M_h = 0.01$), the membrane shape is essentially well-equilibrated during the time scale over which the concentration fields evolve; the dynamics of the membrane fluctuations thus decouples from that of the concentration fields. Hence, the membrane height fluctuations act as a mean field, resulting in a free energy functional in Fourier space that is similar to the one where long-ranged dipolar interactions are important.[10] In the weak segregation limit, where the one wavenumber approximation is valid, these two free energy functionals reduce to exactly the same form, belonging to the Brazovskii universality class.[26] Therefore, it is not surprising that the phase ordering dynamics of these two systems are quite similar (data not shown).

When the membrane fluctuations are relatively slower ($M_\psi/M_h = 1-10$), which is the usual case,[27,28] the dynamics of the membrane and that of the concentration fields are coupled. Although the resulting time scale for the phase ordering dynamics is relatively slower and the domain sizes are much larger than those for model 1, the dynamic features of the phase ordering of the concentration fields (shown in Figure 2) are qualitatively the same as the situation where only long-ranged dipolar interaction is present. The pearling instability could also be explained by a similar analysis as in ref 24 as noted above. Thus, for the incompressible two-component lipid raft model system, model 1 (long-ranged dipolar interactions) and model 2 (spontaneous curvature couplings) lead to phase ordering dynamics that are qualitatively similar. The difference is only that model 2 predicts much larger domain sizes that evolve relatively slowly compared to the results shown in Figure 1 for model 1.

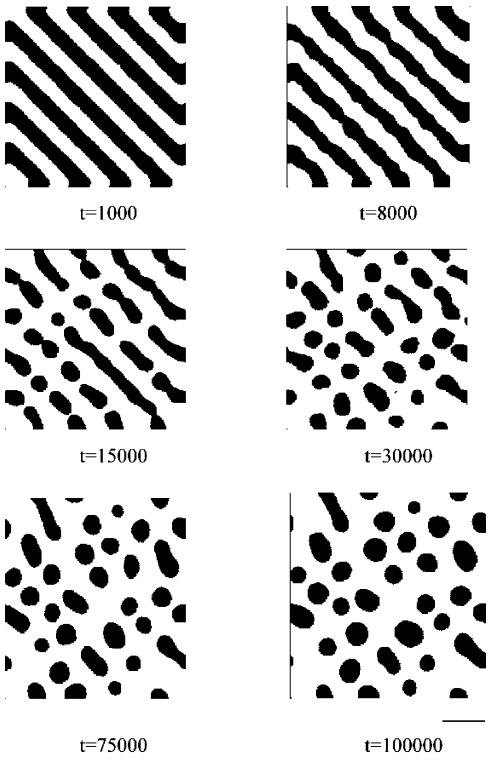

Figure 2. Time evolution of the concentration field for an incompressible two-component lipid raft system upon temperature jump and composition changes. The phase ordering dynamics is based on a lipid raft formation mechanism, which involves coupling of spontaneous curvature differences between components to the concentration fluctuations (model 2). The dark regions are lipid raft domains. t is the simulation time. The characteristic time scales for the concentration field and the membrane fluctuation are chosen to be equal to $M_\psi/M_h = 1$. The temperature jump is instantaneous, from $\tau = -0.25$ to $\tau = -0.01$. The composition is gradually changed from $\rho_A = 0.325$ to $\rho_A = 0.245$. The rate of change of composition is 0.000 001 per simulation time step. The line tension is $\gamma = 4.0k_BT$; the membrane bending modulus is $\kappa = 40k_BT$; the membrane surface tension is $\sigma = 3.1 \times 10^{-6}$ N/m; the spontaneous curvature difference is chosen to be $H_A - H_C = 1.6\ \mu m^{-1}$. The length scale bar is 1500 nm.

Model 3. We simulate the dynamics of the disorder-to-hexagonal-droplet phase transition for the incompressible three-component lipid raft model system. Small random noise (the magnitude is 0.001) is first set as the initial condition for order parameter fields in real space. We equilibrate the system 10 000 time steps at $D_A = 8$ D/nm^2 and $\tau = 0.6$, where the system is well into the disordered phase according to the phase diagram.[10] We then quench the temperature such that the system favors the hexagonal phase ($D_A = 8$ D/nm^2, $\tau = 0.1$).

Parts a and b of Figure 3 show the time evolution of ψ_A and ψ_B in real space, respectively. At early stages, A and B are loosely coupled. B fluctuates over relatively larger length scales than A. During this period, the ordering process for A is faster than that of B. In the intermediate stage, A and B begin to become strongly coupled (the ψ_A field and the ψ_B field are complementary to each other). Now the system starts to exhibit a stripelike morphology (although imperfect) with a characteristic width. The stripes remain there for some period of time. As the ordering process proceeds further, these stripes break

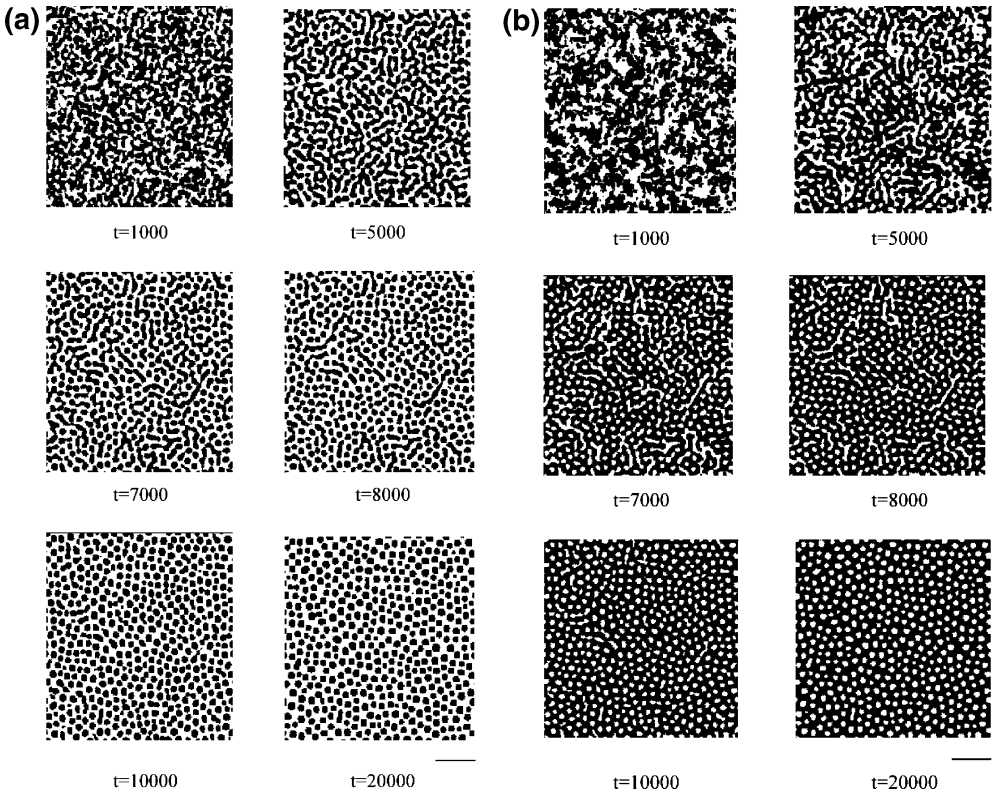

Figure 3. (a) Time evolution of lipid raft domain formation (ψ_A) upon temperature quenching for an incompressible three-component lipid raft system, where long-ranged dipolar interactions are dominant (model 3). The dark regions are lipid raft domains. t is the simulation time. The temperature is quenched from $\tau = 0.6$ to $\tau = 0.1$. The line tension is $\gamma = 5.0k_BT$, $D_A = 8$ D/nm^2, and $D_B = 1$ D/nm^2. The length scale bar is 300 nm. (b) The time evolution of nonraft domains (ψ_B) upon temperature quenching for an incompressible three-component lipid raft system, where long-ranged dipolar interactions are dominant. The dark regions are nonraft domains. t is the simulation time. The temperature is quenched from $\tau = 0.6$ to $\tau = 0.1$. The line tension is $\gamma = 5.0k_BT$, $D_A = 8$ D/nm^2, and $D_B = 1$ D/nm^2. The length scale bar is 300 nm.

up into the hexagonal droplet phase in a manner similar to that of the stripe-to-hexagonal phase transition upon a temperature jump and/or composition change in the incompressible two-component system. The basic dynamic features remain the same if we change the initial states and the final states for the disorder-to-hexagonal phase transition. Thus, the existence of this transient stripe phase appears to be a general dynamic feature for the disorder-to-hexagonal phase transition in the incompressible three-component lipid raft model system.

It is possible that the local anisotropy arising from the initial symmetry breaking drives the concentration fluctuations to first grow in one direction ($\vec{q}_1$), which forms the transient stripelike domain. Later on, as the system progresses toward the global free energy minimum, the hexagonal pattern is acquired through the development of the concentration fluctuation modes in the other two directions ($\vec{q}_2$, $\vec{q}_3$), which satisfy $|\vec{q}_1| = |\vec{q}_2| = |\vec{q}_3| = q$ and $\vec{q}_1 + \vec{q}_2 + \vec{q}_3 = 0$. In this regard, the stripelike phase is more like the bicontinuous pattern occurring at the initial stage of spinodal decomposition in a two-component system. However, in our case, since the three-component system introduces one more degree of freedom, much more complicated intermediate metastable phases that lie between the disordered state and the hexagonal phase could be realized. It would be interesting to see whether this degree of freedom is the origin of the transient stripelike morphology or the stripes are just simply caused by spinodal decomposition as in a two-component system. However, the conventional mode analysis proves to not be very useful in this case, because there is no well-defined global symmetry to start with in the disordered state. We hope to carry out a rigorous analysis in the future.

Concluding Remarks

We have studied the dynamics of order−order and disorder−order phase transitions in models for lipid raft formation in membranes. We studied three models. In all of the models, the system is incompressible, and there is an intrinsic underlying incompatibility between the components that drives phase segregation. Models 1 and 2 contain only two components, while model 3 has three components. In model 1, line tension competes with the effective long-ranged dipolar interactions between membrane components. In model 2, line tension competes with differences in spontaneous curvatures preferred by the different membrane components. The qualitative features of the dynamics of the transition from the stripe to hexagonal droplet phase are similar for both of these models. This is because both models are in the same Brazovskii universality class. The difference between our results for the two models is that the free energy functional in model 1 leads to smaller domain sizes that are similar to the size of lipid rafts on living cell membranes. Our results for models 1 and 2 show that the transition from the stripe to hexagonal droplet phase goes through a pearling instability that is similar to recent experimental observations. It should be noted that this pearling instability during the stripe-to-hexagonal phase transition has also been observed in other quasi-two-dimensional two-component systems.[29,30]

We also studied a three-component system with electrostatic interactions between membrane components in model 3. Specifically, we explored the transition from a disordered phase to the hexagonal phase. We found that dynamic trajectories initially pass through a metastable stripelike phase en route to the

hexagonal droplet phase. We hope that experiments with synthetic systems will be able to test this prediction.

Finally, we would like to point out that, as shown in our previous paper,[10] the equilibrium properties of the lipid raft domains do depend on various physical properties of the components in the lipid raft model system. Similarly, the specific sizes and time scales characterizing the dynamic processes depend on the parameters characterizing the components in our model. However, the generic dynamic features of the phase transitions we have studied here are expected to be independent of these specific parameter values.

Acknowledgment. J.L. thanks Shuyan Qi, Jayajit Das, and Sandy Yang for stimulating discussions and help. Financial support was provided by CIPMA, a NSF funded MRSEC.

References and Notes

(1) Brown, D. A.; London, E. *Annu. Rev. Cell Dev. Biol.* **1998**, *14*, 111.
(2) Simons, K.; Ehehalt, R. *J. Clin. Invest.* **2002**, *110*, 597.
(3) Simons, K.; Ikonen, E. *Nature* **1997**, *387*, 569.
(4) Simons, K.; Toomre, D. *Nat. Rev. Mol. Cell Biol.* **2000**, *1*, 31.
(5) Leibler, S.; Andelman, D. *J. Phys. II* **1987**, *48*, 2013.
(6) Baumgart, T.; Hess, S. T.; Webb, W. W. *Nature* **2003**, *425*, 821.
(7) Veatch, S. L.; Keller, S. L. *Biophys. J.* **2003**, *85*, 3074.
(8) Veatch, S. L.; Keller, S. L. *Phys. Rev. Lett.* **2002**, *89*, 268101.
(9) Keller, S. L.; McConnell, H. M. *Phys. Rev. Lett.* **1999**, *82*, 1602.
(10) Liu, J.; Qi, S. Y.; Groves, J. T.; Chakraborty, A. K. *J. Phys. Chem. B* **2005**, *109* (42), 19960.
(11) Rozovsky, S.; Kaizuka, Y.; Groves, J. T. *J. Am. Chem. Soc.* **2005**, *127* (1), 36. Note that, in this experiment, the composition changes are inferred from the relative coverage of raft domains, where ρ_{raft} changes from 0.325 to 0.245, and we follow exactly the same composition change in our simulations. Throughout the experiment, the GUVs are exposed to radiation which usually causes a small increase in temperature ($\sim$2−3 °C) at the end of the experiment. We took this temperature increase into account by changing the value of our phenomenological Flory−Huggins parameter, τ.
(12) Andelman, D.; Brochard, F.; Joanny, J. F. *J. Chem. Phys.* **1987**, *86*, 3673.
(13) Hohenberg, P. C.; Halperin, B. I. *Rev. Mod. Phys.* **1977**, *49*, 435.
(14) Safran, S. A. *Statistical thermodynamics of surfaces, interfaces, and membranes*; Westview Press: Boulder, CO, 1994.
(15) Lipowski, R. *J. Phys. II* **1992**, *2*, 1825.
(16) Dan, N.; Safran, S. A. *Biophys. J.* **1998**, *75*, 1410.
(17) Bruinsma, R.; Behrisch, A.; Sackmann, E. *Phys. Rev. E* **2000**, *61*, 4253.
(18) Brocca, P.; Cantu, L.; Corti, M.; Favero, E. D.; Motta, S. *Langmuir* **2004**, *20*, 2141.
(19) Murase, K.; Fujiwara, T.; Umemura, Y.; Suzuki, K.; Lino, R.; Yamashita, H.; Saito, M.; Murakoshi, H.; Ritchie, K.; Kusumi, A. *Biophys. J.* **2004**, *86*, 4075.
(20) Dustin, M. L. *J. Clin. Invest.* **2002**, *109*, 155.
(21) Chen, L. Q.; Shen, J. *Comput. Phys. Commun.* **1998**, *108*, 147.
(22) Honig, B. C.; Hubbell, W. L.; Flewelling, R. F. *Annu. Rev. Biophys. Biophys. Chem.* **1986**, *15*, 163.
(23) Brockman, H. *Chem. Phys. Lipids* **1994**, *73*, 57.
(24) Qi, S. Y.; Wang, Z. G. *Phys. Rev. Lett.* **1997**, *76*, 1679. Qi, S. Y.; Wang, Z. G. *Polymer* **1998**, *39*, 4639.
(25) Araki, T.; Tanaka, H. *Phys. Rev. Lett*. **2004**, *93*, 015702.
(26) Brazovskii, S. A. *Sov. Phys. JETP* **1975**, *41*, 85.
(27) Kazushi, Y.; Groves, J. T. *Biophys. J.* **2004**, *86*, 905.
(28) Lipowsky, R.; Sackman, E. *Structure and Dynamics of membranes*; North-Holland: 1995.
(29) Cebers, A. *Braz. J. Phys.* **2001**, *31*, 441.
(30) Sagui C.; Asciutto, E.; Roland, C. *Nano Lett.* **2005**, *5*, 389.